

Electron-beam-induced deposition of 3-nm-half-pitch patterns on bulk Si

J. C. van Oven, F. Berwald, K. K. Berggren,^{a)} P. Kruit, and C. W. Hagen^{b)}
*Delft University of Technology, Faculty of Applied Sciences, Charged Particle Optics Group,
Lorentzweg 1, 2628 C.J Delft, The Netherlands*

(Received 24 June 2011; accepted 25 August 2011; published 20 September 2011)

This paper demonstrates electron-beam-induced deposition of few-nm-width dense features on bulk samples by using a scanning electron-beam lithography system. To optimize the resultant features, three steps were taken: (1) features were exposed in a repetitive sequence, so as to build up the deposited features gradually across the entire pattern, and thus avoid proximity effects; (2) an additional delay was added between exposures to permit diffusion of reactants into the exposed area; and (3) the exposures were phase-synchronized to the dominant noise source (the 50-Hz line voltage) to minimize the effect of noise. The reasons these steps led to significant improvements in patterning resolution are discussed. © 2011 American Vacuum Society. [DOI: 10.1116/1.3640743]

I. INTRODUCTION

Electron-beam-induced-deposition (EBID) is a direct-write lithographic technique that uses a focused electron beam to make small material deposits.¹⁻⁵ By dissociating precursor molecules adsorbed on a surface, two- and three-dimensional structures can be created. The size of these structures can range from single-digit nanometer scale to several micrometers. The minimum feature size possible with EBID is smaller than 1 nm, as has been demonstrated by using finely focused beams in scanning transmission electron microscopes.^{6,7} However, it is more convenient to use the much more user-friendly and widely spread platform of the scanning electron microscope (SEM). We recently demonstrated that EBID can be used to create 3 nm dots in an SEM.⁸ However, deposition was done on a thin membrane and imaging was done using a transmission detector, which, for such small structures, provides better contrast than a secondary electron detector. It was also found that, when decreasing the separation between deposits, they became broader. This broadening is due to proximity effects. There are two proximity effects that play a role here. First, the angular dependence of the secondary electron (SE) yield, which causes the growth rate to increase when the beam irradiates the slope of the deposit.^{9,10} This results in nonlinear growth when writing EBID lines consisting of overlapping dot exposures. Second, during deposition of a line, secondary electrons escaping from that line may dissociate precursor molecules on the neighboring line, causing it to grow further.¹¹⁻¹³

The challenge we address now is to pattern lines and spaces, as densely as possible, on bulk material as opposed to a membrane. This challenge is important for applications in the fields of mask repair and circuit edit, as well as nano-scale prototyping. Working on bulk material forces us to use

SE detection for imaging the patterns, and to develop a strategy to deal with the proximity effects. We will demonstrate the fabrication of dense patterns on a sub-10 nm scale on bulk silicon substrates using EBID.

II. EXPERIMENT

The EBID setup we used is an FEI Quanta 3D FEG Dual Beam machine, with a 30 keV electron beam energy and a smallest specified probe size of ~ 1.2 nm with 6 pA of current. We used the standard gas injection system with methylcyclopentadienyl(trimethyl)platinum (MeCpPtMe₃, CAS: 94442-22-5) as a precursor gas. The precursor molecules enter the vacuum chamber through a nozzle that was either located 50 μm above the substrate surface, or a few centimeters away from the substrate, when patterning at small working distance. The background vacuum of the specimen chamber was $\sim 2 \times 10^{-6}$ mbar. With the nozzle opened, the chamber pressure rose to $\sim 1.2 \times 10^{-5}$ mbar. The EBID patterning was done either by using the FEI Graphical User Interface or by using home-built, LABVIEWTM-based, patterning software. The highest spatial resolution is expected to be obtained with the smallest probe size. Therefore, the highest accelerating voltage of 30 kV was combined with the smallest probes, with beam currents ranging from 6 to 24 pA. The substrates the patterns were deposited onto were polished p-doped (1–50 $\mu\Omega\text{cm}$) 200- μm -thick silicon wafers.

The pattern used for the dense lines and spaces was a nested-L structure, consisting of seven closely spaced L-shaped lines. The center line was longer than the others, such that dense lines and spaces, and isolated lines, were fabricated simultaneously. This allowed for an easy comparison between the deposition of an isolated line, and the deposition of lines in close proximity of each other. Of the outermost L-shaped lines, we call the shortest line the inner line, and the longest line the outer line. Writing an L-shaped pattern, requires both scan directions of the electron beam, and therefore reveals beam astigmatism. All patterns were written line by line, starting with the outer line of the nested-L and finishing with the inner line. Apart from nested-L's, we also

^{a)}On leave from Research Laboratory of Electronics, Massachusetts Institute of Technology, 77 Massachusetts Avenue, Cambridge, Massachusetts 02139.

^{b)}Electronic mail: c.w.hagen@tudelft.nl

patterned slightly more complex structures to demonstrate the lithographical capabilities of EBID.

Inspection of the structures was done in SE mode in the same SEM that we used for patterning. To reduce noise during analysis of the images, we created integrated line profiles by averaging the signal intensity of the image in the direction of the lines. We then fitted the integrated line profiles with a sum of seven Gaussian distributions, one for each EBID line. From the fits, we calculated the full-width at half maximum (FWHM) for each line. Because the SE signal is not linear with the amount of deposited material, the FWHM found this way does not necessarily correspond to the actual FWHM of the deposit. However, the pitch between the lines can be precisely determined by this approach.

III. RESULTS AND DISCUSSION

Our goal was to test the limits of EBID lithography on the smallest pattern possible, focusing on both feature size and shape, which are influenced by the precursor density on the sample, the electron flux, and the writing strategy.

A first series of experiments was aimed at controlling the proximity effects mentioned before. L-shaped patterns were written in a single pass with a 30 kV electron beam, a beam current of around 24 pA, and the total linear dwell time was 30 ms/nm (0.72 pC/nm total line dose). The resulting patterns had a pitch of 30 nm and are shown in Fig. 1(a). We clearly observe the two proximity effects. The nested-L's were written line by line, from outer to inner line, each line was written top down and then from left to right. Each line was seen to start small, but due to the angular dependence of the SE yield, the growth rate increased over time (the first proximity effect). It was also observed that the dense lines were wider than the isolated line parts. The deposition on neighboring structures explains this difference (the second proximity effect). To correct for both types of proximity effects, in a second series of experiments, the pattern was built up in multiple passes. That is, the entire pattern was written 300 times, each time starting with the outer line and finishing with the inner line, keeping the total line dose, pitch and the SEM settings the same, so that each pass used a reduced dose. By doing so, the pattern was built up more homogeneously and the SE yield was kept low at all times. The image of the proximity-corrected pattern is shown in Fig. 1b. Notice not only that the nonlinearities have disappeared, but also that the total amount of deposit was smaller when doing multiple passes, presumably because the SE yield was kept low at all times. In all subsequent experiments patterns were written with at least 300 passes.

By lowering the dose and adjusting the pitch, we were able to write lines and spaces with a pitch of 10 nm. At this point, a new phenomenon appeared. In contrast to what was expected, and observed when doing a single pass pattern, the isolated lines now grew broader than the dense lines. The same phenomenon was observed for the outermost lines of the nested-L structure. This effect is clearly visible in Fig. 2.

After some optimization of the dose, we were still unable to achieve a pitch below ~ 9 nm. To understand possible rea-

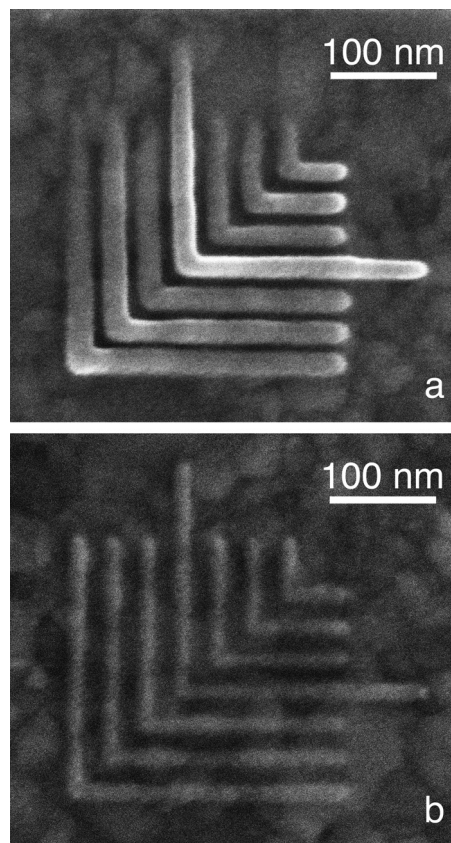


FIG. 1. Correction of proximity effects: (a) EBID of a nested-L with a pitch of 30 nm on silicon with a layer of gold. This pattern was built up in one pass by a 30 kV beam, spot 4 and a total linear dwell time of 30 ms/nm (0.72 pC/nm total line dose). The pattern was written line by line, top down and from left to right. Both proximity effects described above are visible. Due to the angular dependence of the SE yield, a single line started small at the top and grew during the write. The isolated line is smaller than the dense lines. The absence of the deposit of neighboring structures explains this feature size bias. (b) Another nested-L was written with the same SEM settings. To correct for the proximity effects visible in (a), the write was divided into 300 passes. Notice not only that the nonlinearities have disappeared, but also that the total amount of deposit was smaller when doing multiple passes, presumably because the SE yield was kept low at all times.

sons for this limit, it is useful to think about what parameters contribute to the deposit size and growth rate. In a simple picture, the size should be approximately equal to the probe size of the beam, which is ~ 1 nm. However, SE's are also believed to contribute in the dissociation process.¹⁴ Therefore, the SE-emission area, with a radius of ~ 1 nm, causes some broadening of the deposits.¹⁵ When a spot is irradiated for a longer time, scattering of electrons inside the deposit, generating secondary electrons escaping from the sidewalls of the deposit, cause it to grow, not only in height but also in width.¹⁶ This effect makes the dose an important variable when doing high resolution EBID. The growth rate and shape are also highly dependent of the precursor surface density. Depletion of precursor molecules leads to slow growth and flat shapes, while a high precursor density leads to fast growth and steep features. For a comprehensive review on EBID growth shapes we refer to the work of Utke.¹

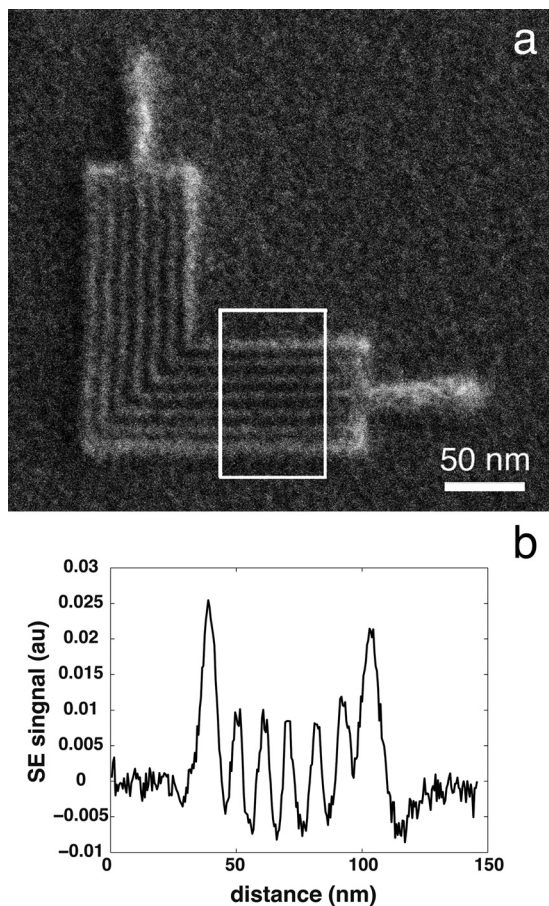


FIG. 2. Broadening caused by precursor depletion and diffusion. (a) A 10-nm-pitch nested-L written on silicon (30 kV, spot 4, 27 ms/nm, 0.65 pC/nm total line dose, 325 passes). The broad isolated line parts and outer lines indicate that EBID was in the diffusion enhanced regime. (b) An integrated line profile from the lines inside the box in (a) shows clearly the difference between the outer lines and the inner lines.

So, in theory, smaller feature sizes than the ones we created should be possible. We suspected that vibrations, or other disturbances, in our system caused resolution loss. To check this hypothesis, we imaged a straight edge with a short scan time (1 μ s pixel dwell time, and a line scan time of 2.048 ms). The apparent disturbances appeared as standing waves in the image shown in Fig. 3. Two oscillations with different frequencies and amplitudes are visible in the image. We suspect that the 7 Hz oscillation had a mechanical cause. The high frequency oscillation had a frequency of 50 Hz, that appeared to be exactly in sync with the power line, and was probably caused by oscillating magnetic fields inside the SEM. Mechanical vibrations can be reduced by better damping and isolation of the system. However, the magnetic disturbances, that were in sync with the phase of the mains power supply, were harder to remove. Because the source of this oscillation is unknown and possibly inside the machine, it is impossible to shield the electron beam from this field, and another approach had to be used to reduce the EBID quality loss caused by this disturbance. The patterns were built up in multiple passes and the time each pass took was of the same order as the period of the power line. The vibration in one pass therefore resulted in a barely visible wobble,

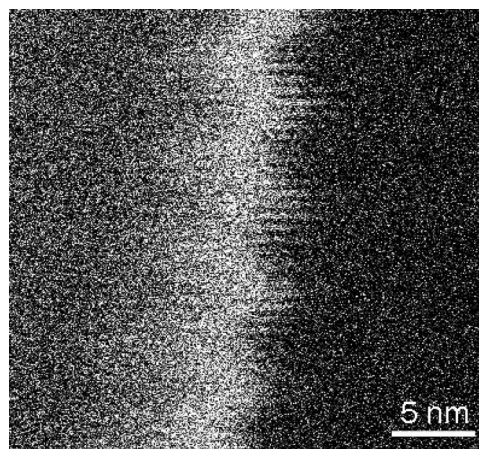


FIG. 3. To measure disturbances in the system, we imaged a sharp edge with a short scan time to make the oscillations appear as standing waves. Two oscillations, 50 Hz and 1.3 nm amplitude, and 7 Hz with 1 nm amplitude, are visible. The pixel dwell time was 1 μ s and the line scan time was 2.048 ms.

spread out through the entire nested-L. Because the phase of the vibration is shifted a bit each pass, lines written this way will suffer resolution loss. By synchronizing the writing sequence to the phase of the power line, the time varying shift of the phase of the vibration could be eliminated. With this synchronization, the beam would follow exactly the same path each pass and the vibration should not influence EBID resolution.

During patterning, the phase of the power line was measured with external hardware. After each pass, the beam waited at a parking position until it was triggered by the external hardware to make the next pass. The time the beam had to wait was dependent on the time a pass took and varied from 0 to 20 ms (one period of the power line). Due to sampling limitations of the data acquisition boards in our setup, synchronization with the power line was done only during writing of EBID structures, and not during imaging of the structures.

This patterning strategy resulted in structures where the irregularities, shown in Fig. 2, were less apparent. We soon suspected that not only was the suppression of the oscillation causing this improvement, but the waiting time between passes also had an impact. To test these assumptions, two further experiments were done.

In the first experiment, only the influence of the waiting time was investigated. In Fig. 4, two nested-L structures are shown. Both have a pitch of 10 nm, and were written on a silicon substrate with a 30 kV beam, beam current of around 24 pA, 50 ms/nm line dwell time, a total line dose of 1.2 pC/nm, and were built up in 300 passes. In Fig. 4(a), no waiting time between passes was implemented, but in Fig. 4(b), a waiting time of 150 ms between passes was applied. The waiting time resulted in a huge improvement in EBID quality. The broad outer regions in Fig. 4(a) (that we also saw in Fig. 2) disappeared and the entire pattern became more uniform. This improvement can be explained by precursor migration.^{17–19} Because these high-resolution experiments required a short working distance (\sim 3 mm), the precursor

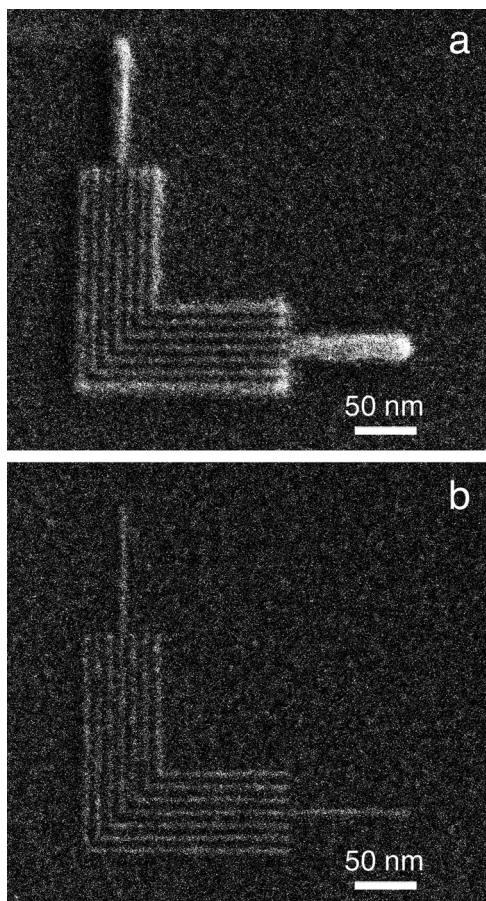


FIG. 4. Comparison of two 10-nm-pitch nested-L patterns written on silicon (both 30 kV, spot 4, 50 ms/nm linear dwell time, 0.32 pC/nm total line dose, 300 passes) to demonstrate the influence of the waiting time between passes. During the waiting time, precursor molecules diffuse into the depleted areas, this leads to more uniform structures. (a) No waiting time between passes, (b) a waiting time of 150 ms was implemented after each pass.

supply nozzle had to be retracted. We hypothesize that therefore the EBID growth was limited by the precursor supply, and precursor replenishment was dominated by diffusion. After a pass of the electron beam, the surface was locally depleted and precursor molecules diffused from the area around the pattern to the depleted areas. This depletion created a gradient in surface density of precursor molecules; with lower surface density, and therefore lower growth rate, toward the pattern center. When the number of incoming electrons was very high compared to the number of precursor molecules, and passes followed each other very quickly, almost all precursor molecules dissociated in the outer regions of the nested-L before they reached the center, and therefore growth of the center lines was limited. Similar results, where the combination of depletion and diffusion caused volcano shaped deposits, were obtained in practice²⁰ and in simulation.²¹ However, with a waiting time between passes, precursor molecules had time to diffuse to depleted areas, which resulted in a higher, and more uniform, surface density during the next pass at all positions. This uniformity led to taller lines and more uniform patterns, as shown in Fig. 4(b). Although this hypothesis explains why the inner lines of the nested-L grew faster, it does not explain why the edges and isolated parts appear to have become smaller due to the waiting time. To answer this question, further investigation is needed.

In the second experiment, we tested whether synchronization of each pass with the power line increased the EBID quality. Two more nested-L structures were written on a silicon substrate, with a 30 kV beam, spot 1, 34 ms/nm total line dwell time, 0.21 pC/nm total line dose, and 500 passes. In both patterns, a waiting time was added after each pass of 20 ms, to allow for sufficient precursor replenishment. The first pattern, part of which is shown as the left hand inset of Fig. 5, was written without synchronization, and the second pattern, part of which is shown as the right hand inset of

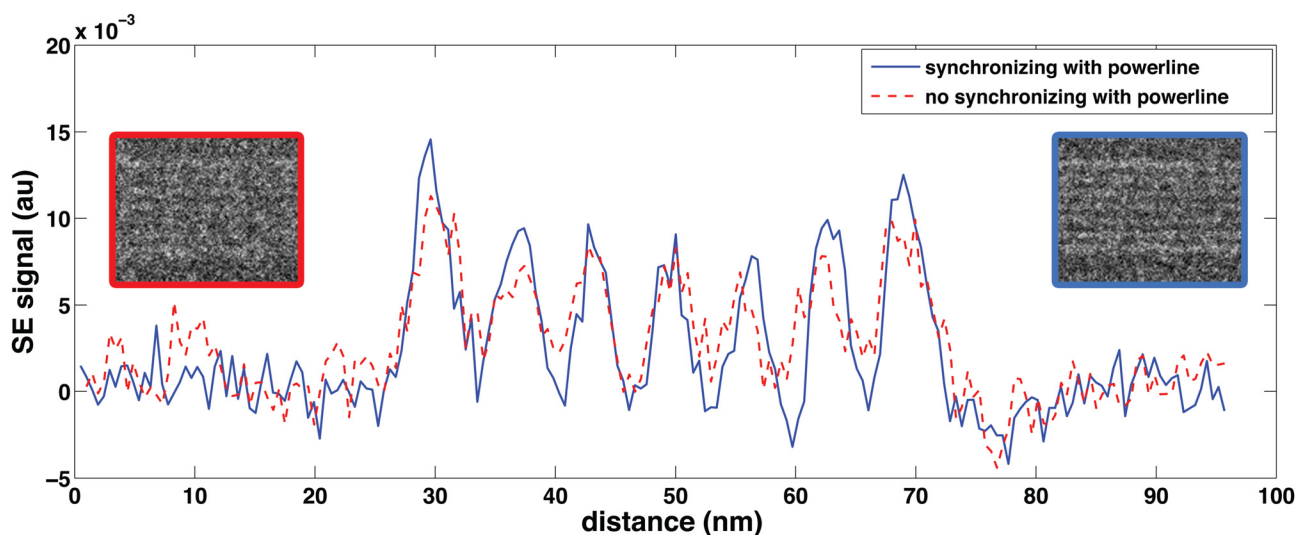


FIG. 5. (Color online) Comparison of two integrated line profiles of 7.6-nm-pitch dense lines. The blue integrated line profile (the drawn line) was patterned synchronized to the power line, resulting in a sharper line profile than the red integrated line profile (the dashed line) that was taken from unsynchronized lines. The patterned horizontal lines (left unsynchronized, right synchronized) are shown in the insets. The lines are written on silicon (30 kV beam, spot 1, 34 ms/nm total line dwell time, 0.21 pC/nm total line dose and 500 passes with 20 ms additional waiting time after each pass).

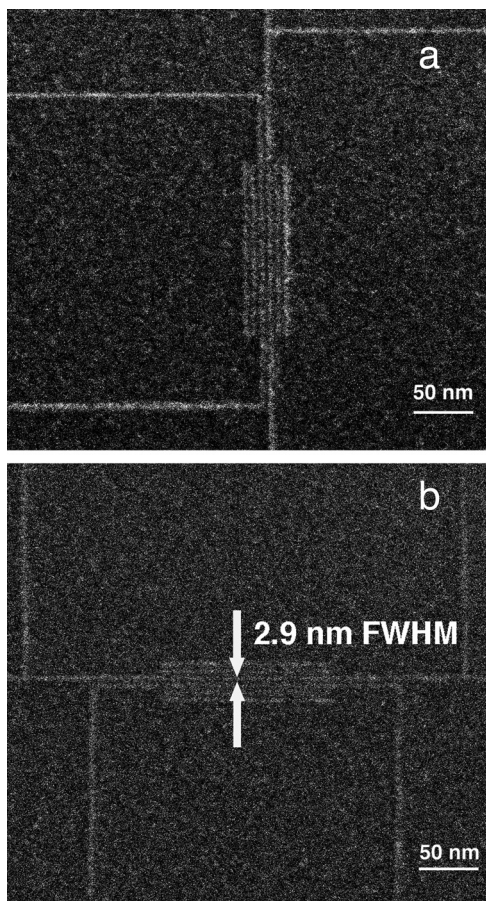


Fig. 6. Two more complex structures, written on silicon, with contact wires, appropriate for resistivity measurements, demonstrate the capability of EBID as a high-resolution patterning technique. Both structures were written with the same SEM settings (30 kV beam, spot 4, 40 ms/nm linear dwell time, 0.96 pC/nm total line dose, 3 mm working distance, 500 passes, synchronized with the power line, and with a 100 ms pause after each pass). (a) A structure showing isolated and dense lines with a pitch of 7 nm. (b) In this structure the pitch between the lines in the dense part is 6 nm. The smallest line indicated with the arrows has an average width of 2.9 nm FWHM.

Fig. 5, was written synchronized with the power line. The pitch between the lines was 7.6 nm. The improvement caused by synchronization can best be seen by comparing the integrated line profiles of both patterns shown in Fig. 5. The center part of Fig. 5 shows the two integrated line profiles. The synchronized pattern clearly shows higher-contrast lines, of smaller width.

By combining the three patterning strategies, multiple passes, a waiting time between passes and 50-Hz synchronization, we were able to fabricate structures that show the true potential of EBID as a high resolution lithography tool. In Fig. 6, two patterns can be seen, all written with the same SEM settings (30 kV beam, beam current of around 24 pA, 40 ms/nm total line dwell time, 0.96 pC/nm total line dose, 3 mm working distance, 500 passes and synchronized with the power line, and with a 100 ms pause after each pass), but with different pitch between the dense lines. The pitches of Fig. 6(a) and 6(b) are 7 and 6 nm, respectively. Future measurements will have to reveal whether the electrical conductivity of these structures is good enough for applications.

It is well-known that EBID lines, as deposited from the MeCpPtMe₃ precursor, may contain about 80% of carbon.²² This can be reduced in post-deposition treatments, improving the conductivity by several orders of magnitude.^{22,23} Alternatively, these ultra-small EBID structures can be applied as etch masks^{24,25} to be used for pattern transfer into an underlying pure metal layer.

It is important to keep in mind that the SE yield is angle dependent and not linear with the amount of material that is deposited. Definitive conclusions about the deposit sizes are therefore hard to draw. Other imaging techniques such as high-angle annular dark field imaging (HAADF) in scanning transmission electron microscopy (STEM) (limited to thin samples, but with the signal being proportional to the amount of deposited material) or atomic force microscopy (AFM) could provide more information about the deposit dimensions, and will be considered in future work.

IV. CONCLUSIONS

In conclusion, our goal was to use EBID to deposit dense lines and spaces on bulk samples in an SEM and image the structures with the same SEM in SE mode. We created dense lines and spaces with a pitch of 6.1 nm, and an average line-width of 2.9 nm (FWHM), as measured in the SEM. This pattern was achieved by combining a multiple passes writing strategy, to reduce proximity effects, with a waiting time between passes, to enhance precursor replenishment, and synchronization of the writing to the power line, to reduce blurring caused by magnetic disturbances.

ACKNOWLEDGMENTS

K.K.B. acknowledges the support by the Dutch Organisation for Scientific Research NWO (Nederlandse Organisatie voor Wetenschappelijk Onderzoek), and C.W.H. acknowledges the support provided by the EU Cost Action CM0601 “Electron Controlled Chemical Lithography” (ECCL).

- ¹I. Utke, P. Hoffmann, and J. Melngailis, *J. Vac. Sci. Technol. B* **26**, 1197 (2008).
- ²N. Silvis-Cividjian and C. W. Hagen, *Adv. Imaging Electron Phys.* **143**, 1 (2006).
- ³W. F. van Dorp and C. W. Hagen, *J. Appl. Phys.* **104**, 081301 (2008).
- ⁴M. Song and K. Furuya, *Sci. Technol. Adv. Mater.* **9**, 023002 (2008).
- ⁵S. J. Randolph, J. D. Fowlkes, and P. D. Rack, *Crit. Rev. Solid State Mater. Sci.* **31**, 55 (2006).
- ⁶W. F. van Dorp, B. van Someren, C. W. Hagen, P. Kruit, and P. A. Crozier, *Nano Lett.* **5**, 1303 (2005).
- ⁷W. F. van Dorp, C. W. Hagen, P. A. Crozier, and P. Kruit, *Nanotechnology* **19**, 225305 (2008).
- ⁸L. van Kouwen, A. Botman, and C. W. Hagen, *Nano Lett.* **9**, 2149 (2009).
- ⁹W. F. van Dorp, S. Lazar, C. W. Hagen, and P. Kruit, *J. Vac. Sci. Technol. B* **25**, 1603 (2007).
- ¹⁰P. A. Crozier, *J. Vac. Sci. Technol. B* **26**, 249 (2008).
- ¹¹Y. M. Lau, P. C. Chee, J. T. L. Thong, and V. Ng, *J. Vac. Sci. Technol. A* **20**, 1295 (2002).
- ¹²D. J. Burbridge and S. N. Gordeev, *Nanotechnology* **20**, 285308 (2009).
- ¹³K. Mitsuishi, M. Shimojo, M. Takeguchi, M. Tanaka, and K. Furuya, *Jpn. J. Appl. Phys.* **45**, 5517 (2006).
- ¹⁴C. W. Hagen, W. F. van Dorp, P. A. Crozier, and P. Kruit, *Surf. Sci.* **602**, 3212 (2008).
- ¹⁵N. Silvis-Cividjian, C. W. Hagen, and P. Kruit, *J. Appl. Phys.* **98**, 084905 (2005).

- ¹⁶N. Silvis-Cividjian, C. W. Hagen, L. H. A. Leunissen, and P. Kruit, *Microelectron. Eng.* **61–62**, 693 (2002).
- ¹⁷M. Amman, J. W. Sleight, D. R. Lombardi, R. E. Welser, M. R. Deshpande, M. A. Reed, and L. J. Guido, *J. Vac. Sci. Technol. B* **14**, 54 (1996).
- ¹⁸H. Plank, C. Gspan, M. Dienstleder, G. Kothleitner, and F. Hofer, *Nanotechnology* **19**, 485302 (2008).
- ¹⁹J. D. Fowlkes and P. D. Rack, *ACS Nano* **4**, 1619 (2010).
- ²⁰I. Utke, V. Friedli, M. Purrucker, and J. Michler, *J. Vac. Sci. Technol. B* **25**, 2219 (2007).
- ²¹D. A. Smith, J. D. Fowlkes, and P. D. Rack, *Nanotechnology* **19**, 415704 (2008).
- ²²A. Botman, M. Hesselberth, and J. J. L. Mulders, *Microelectron. Eng.* **85**, 1139 (2008).
- ²³A. Botman, J. J. L. Mulders, and C. W. Hagen, *Nanotechnology* **20**, 372001 (2009).
- ²⁴C. Th. H. Heerkens, J. M. Kamerbeek, W. F. van Dorp, C. W. Hagen, and J. Hoekstra, *Microelectron. Eng.* **86**, 961 (2009).
- ²⁵Y. Guan, J. D. Fowlkes, S. T. Retterer, M. L. Simpson, and P. D. Rack, *Nanotechnology* **19**, 505302 (2008).